Scilight

Photochemistry and Spectroscopy
https://www.sciltp.com/journals/ps

Article

Using Surface Phonons as a Guide for Optimizing SERS and Light-Driven Processes †

Ivano Alessandri [1,2,3]

[1] Information Engineering Department, University of Brescia, via Branze 38, 25123 Brescia, Italy; ivano.alessandri@unibs.it
[2] Research Unit of Brescia, Consorzio Interuniversitario per la Scienza e Tecnologia dei Materiali, INSTM, via Branze 38, 25123 Brescia, Italy
[3] Research Unit of Brescia, CNR-INO, via Branze 45, 25123 Brescia, Italy

† This article is dedicated to Prof. Giuseppe Zerbi in recognition of his outstanding scientific contributions to Spectroscopy.

How To Cite: Alessandri, I. Using Surface Phonons as a Guide for Optimizing SERS and Light-Driven Processes. *Photochemistry and Spectroscopy* **2026**, *2*(2), 5. https://doi.org/10.53941/ps.2026.100016

Received: 15 December 2025
Revised: 3 March 2026
Accepted: 4 March 2026
Published: 7 May 2026

Abstract: The characterization of surface plasmon–polaritons (SPPs) involved in surface-enhanced Raman scattering (SERS) and plasmon-driven photochemical processes is commonly performed through auxiliary techniques such as optical-, electron energy loss- or scanning probe-spectroscopy that neither reproduce the actual excitation conditions of a microRaman setup nor provide a direct, in situ probe of light confinement in real experiments. Here, we demonstrate an alternative approach based on the intrinsic Raman response of TiO_2 hollow-shell cavities coated with ultrathin gold layers (T-horex@Au). The Raman spectra of these hybrid core/shell structures exhibit an additional mode that cannot be assigned to bulk TiO_2 phonons. Confocal microRaman analysis reveals a clear dependence of this mode's intensity on the laser penetration depth, enabling its attribution to surface phonon modes activated at the Au/TiO_2 interface. This plasmon-mediated activation takes advantage of interfacial symmetry lowering and efficient electromagnetic field confinement. The simultaneous observation of this mode together with conventional Raman signals provides a direct, non-perturbative diagnostic of SPP excitation quality under realistic experimental conditions. Exploiting this feature, we show that the Raman enhancement induced by identical gold layers is strongly substrate-dependent and that the intensity of the TiO_2 surface mode can be used as an internal standard to optimize and tune SERS performance. This strategy offers a practical route for large-scale fabrication and rapid optimization of metal/TiO_2-based SERS substrates, opening intriguing perspectives for real-time control and monitoring of plasmon-driven photocatalytic and photochemical reactions at solid interfaces.

Keywords: TiO_2; surface phonons; surface plasmon polaritons; SERS; photocatalysis

1. Introduction

Plasmonic materials are widely investigated as substrates for promoting surface enhanced Raman scattering (SERS) and photochemical reactions [1–3].

In particular, the Au–TiO_2 system represents an important subject of study in photocatalysis, as it is employed in a wide variety of reactions and plasmon-assisted processes, such as CO_2 photoreduction [4] or the selective photooxidation of CO [5] and alcohols [6], the degradation of organic pollutants and pathogens [7], water splitting and hydrogen evolution reaction [8], C–C [9] coupling reactions, etc. A large fraction of these processes is based on the mediation of surface plasmon polaritons, which play a key role in the excitation of hot carriers and/or in the promotion of photothermal effects. In the field of SERS, the Au/TiO_2 system has attracted considerable interest in recent years in the context of photo-induced enhanced Raman spectroscopy (PIERS) [10]. TiO_2 alone has also

proven to be a key factor in enhancing the Raman signal in core/shell structures used for Raman signal amplification based on the combination of geometric effects and Mie-type modes [11–16].

Combining TiO_2-based dielectric resonators (T-rex or T-horex) [11] with thin films of plasmonic materials, such as Au, could therefore prove extremely interesting both from a photocatalytic perspective-as already demonstrated by the combined use of plasmonic nanoantennas integrated into TiO_2 nanoshells [17]-and from the standpoint of SERS.

However, the characterization of the signal associated with surface plasmon–polaritons utilized to amplify the Raman effect and/or drive certain photochemical reactions cannot be carried out directly during the acquisition of a Raman spectrum, but typically requires separate characterization based on visible spectroscopy or electron energy loss spectroscopy (EELS) [18].

In addition to the need for preliminary characterization-which therefore requires additional time and resources-both of these methods share the fundamental disadvantage of not accurately reproducing the plasmonic excitation conditions that occur in a SERS or plasmon-driven photochemistry experiment. In fact, the characterization of the metallic surface or the metal/semiconductor interface in the far-field does not accurately reflect the situation that occurs at the nanoscale, unless scanning near field optical spectroscopy (SNOM) or other tip-enhanced spectroscopy approaches are used, which however entails a significant perturbation of the local electromagnetic field. Likewise, EELS requires operation under ultra-high vacuum, with obvious operational drawbacks [19].

This work analyzes the Raman signal of TiO_2 hollow-shell cavities coated with ultrathin layers of Au (T-horex@Au). The Raman spectrum of these core/shell structures reveals the presence of a mode that cannot be attributed to the phonon modes of TiO_2. A more in-depth characterization, based on confocal microscopy, highlights a dependence of the intensity of this mode on the penetration depth of the Raman beam, allowing it to be correlated with the presence of surface plasmon polaritons at the TiO_2/Au interface and their ability to coupling with the surface phonons of TiO_2. The observation of this mode within the same spectral output as the Raman signals provides a direct diagnostic of the quality of light confinement at the sample surface, enabling optimization of the analytical conditions of a Raman experiment or, prospectively, allowing control over the progress of a photocatalytic reaction on the surface of these materials.

2. Experimental

2.1. Fabrication of T-Horex, T-Horex@Au Beads and Au-on-Glass Slide References

The T-horex beads utilized as substrates for the deposition of Au thin films were fabricated as follows: 2-μm-sized monodispersed polystyrene (Microparticles GmbH) beads were drop casted on the surface of silicon (100) supports. Upon drying and ozone-UV cleaning they were coated with a 100-nm thick layer of amorphous TiO_2 by atomic layer deposition (Savannah 100-Cambridge Nanotech Inc., Walthman, MA, USA), following the same protocol utilized for preparing SiO_2/TiO_2 core/shell resonators (T-rex) in previous works [11,12]. Briefly, tetrakisdimethyl-amido titanium (TDMAT; purity 99.999%, Aldrich, Schellendorf, Germany) was utilized as the titanium source and water as the oxygen source. The deposition temperature and pressure were 90° C and 0.5 Torr, respectively. Nitrogen was used as a precursor carrier and purge gas.

The as-prepared core/shell beads were annealed in air at 700 °C for 4 h, with a ramp of 2 °C/min, resulting in hollow TiO_2 shells (T-horex).

The thermally treated beads served as support for the dc-sputtering deposition (K550 sputtering coater, discharge current: 35 mA, total pressure: 10^{-1} mbar, room temperature) of two different thin layers of Au, with nominal thickness of 8 and 16 nm, respectively (T-horex@Au).

The overall sequence of the fabrication steps is shown in Figure 1.

Reference samples were prepared by depositing 8-nm thin films on microscope glass slides previously cleaned in a water/acetone and treated in ozone-UV-cleaner at 50 °C for 10 min.

The morphology of the resulting T-horex@Au was checked by Scanning Electron Microscopy (Leo Evo 40XVP).

The optical reflectance in Visible of both T-horex and T-horex@Au was measured by a QE65000 Ocean Optics spectrometer.

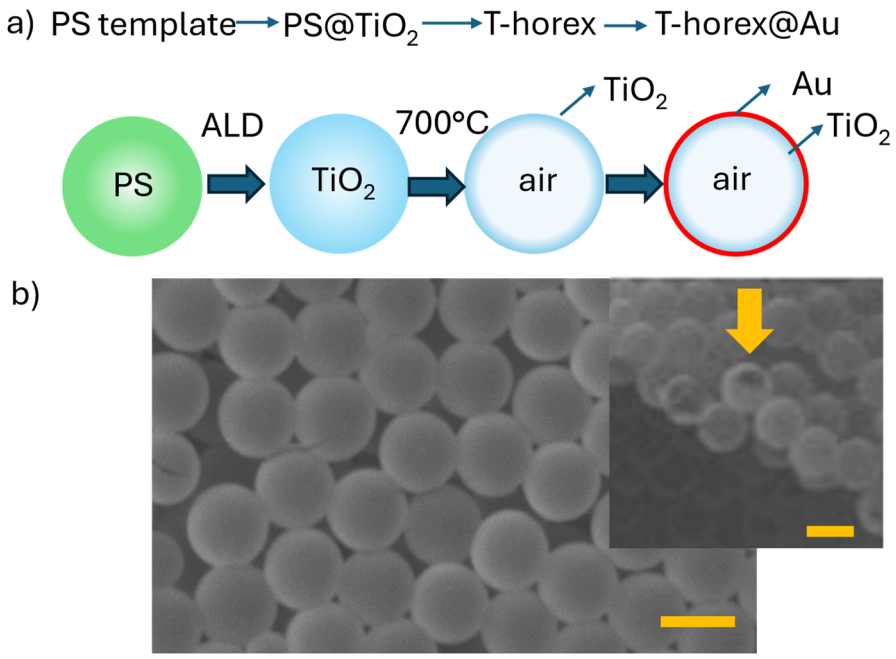

Figure 1. (**a**) Scheme of the fabrication of T-horex@Au core/shell beads; (**b**) SEM image of T-horex@Au beads. In the inset, a scratched bead, indicated by the arrow, shows the hollow core resulting from the removal of the PS template. Scale bars: 2 µm.

2.1. Confocal microRaman Characterization

The MicroRaman characterization of T-horex@Au was carried out with a confocal Labram HR-800 (Horiba-Jobyn Yvon, Kyoto, Japan). The specific acquisition conditions of the different experiments are reported in the main text and in the captions of the corresponding figures. At least 10 different T-horex@Au beads were probed for each series of measurements. The relative standard deviation (RDS) in all the series was <5%.

The experiments of L-Cysteine detection were carried out by soaking either the T-horex@Au or the Au on glass substrates in a L-Cysteine 10^{-4} M water solution overnight. The substrates were extracted, thoroughly washed three times in ultrapure water to remove the excess of L-Cysteine and dried under a gentle N_2 flow and measured immediately.

3. Results and Discussion

3.1. Confocal Microraman Characterization of T-Horex and T-Horex@Au

Figure 2 (panel a) shows the comparison between the Raman spectra of T-horex and T-horex@Au samples acquired under the same conditions (1 s, objective numerical aperture, N.A.: 0.5).

Both the spectra show the Raman-active modes typical of anatase-type TiO_2 (E_{g1}: 143 cm^{-1}, E_{g2} = 196 cm^{-1}, B_{1g}: 399 cm^{-1} A_{1g} + B_{1g2}:518 cm^{-1} and E_{g3}: 638 cm^{-1}) [11], however the intensity of the T-horex@Au spectra is remarkably reduced in comparison to that of the T-horex counterpart, indicating that the Au shell effectively shields the penetration of the laser beam. On the other hand, the background in the presence of Au is significantly increased because of photoluminescence, which is characteristic of Au nanolayers [20,21].

Interestingly, when optical filters were utilized to reduce the power of the laser released on the sample surface a new Raman mode appeared at around 700 cm^{-1}, corresponding to 662 nm (1.87 eV), which was not observed in the absence of Au (Figure 2, panel b, upper).

The mode is quite broad, and its relative intensity increases progressively as a function of the power attenuation, as confirmed also by the CCD images (Figure 2 panel 2b, lower and Supporting Information Figure S1), suggesting its relationship with the Au surface layer. The mode remained unchanged after multiple acquisitions, confirming that its origin is not photothermal (Supporting Information Figure S2), as expected from the inverse dependence of the intensity on the laser power.

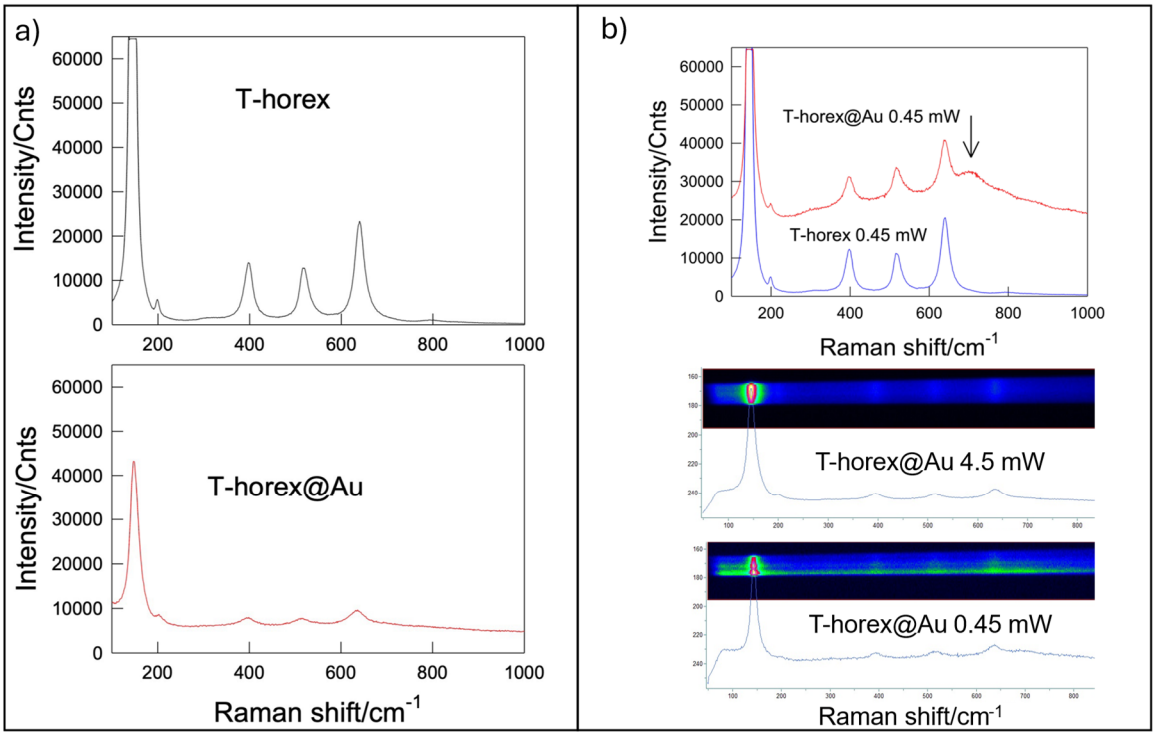

Figure 2. (**a**): Comparison between the Raman spectra of T-horex and T-horex@Au acquired by exciting the samples with a He-Ne laser at 632.8 nm at the power of 4.5 mW, photon flux: 1.43×10^{16} photons/s for 1 s through a 50 Long Working Distance (LWD) objective (numerical aperture, N.A.: 0.5). (**b**), upper: Comparison between the Raman spectra of T-horex and T-horex@Au acquired by exciting the samples with a He-Ne laser at 632.8 nm at the power of 0.45 mW, photon flux: 1.43×10^{15} photons/s for 10 s through a 50 Long Working Distance (LWD) objective (numerical aperture, N.A.: 0.5). (**b**), lower: CCD image of the same T-horex@Au sample acquired for 1 s at 4.5 and 0.45 mW, respectively.

Figure 3a shows a comparison among the spectra acquired on the same T-horex@Au with different microscope objectives at the same exposure time. The intensity of the mode at 700 cm^{-1} revealed a clear dependence on numerical aperture of the microscope objective, being hardly detectable at the lowest numerical apertures, while significantly increasing its relative intensity at higher numerical apertures, which reduce laser penetration, allowing for better surface sensitivity. Figure 3b shows the equivalent of a z-scan acquisition achieved by progressive attenuation of the laser power focused through the highest numerical aperture (0.9) microscope objective. Again, the progressive increase of the intensity of the 700 cm^{-1} mode and a slight, yet significant (−5 cm^{-1}) shift of the band maximum is observed as function of power attenuation, on passing from 2.25 to 1.125 mW. Moreover, the shape of this mode becomes progressively more symmetric (see also Supporting Information Figure S3). A quantitative evaluation of this effect is reported in graph of Figure 3c. Taking the TiO_2 E_{g3} mode at 638 cm^{-1} as a reference, we can observe a I_{638}/I_{700} cm^{-1} ratio of about 3.5 for the maximum laser power, whereas this ratio approaches 1 (1.16) at the lowest power. This analysis confirms that the mode at 700 cm^{-1} originated from interaction of light with the gold surface.

The dependence of this mode on the energy of the exciting laser was investigated by acquiring Raman spectra using laser sources at 532 and 785 nm.

As observed in Figure 4a, the excitation at 532 nm does not allow to excite this mode, whereas the mode is detectable with the 785 nm source (Figure 4b), yet very weak in comparison to that observed at 633 nm, as clearly observed in Figure 4c. A closer inspection in the Raman spectrum of T-horex@Au samples excited at 785 nm shows a remarkable reduction of the Raman background. The fact that this background reduction is observed also for sample irradiated at 532 nm, i.e., at an energy value that are higher than that of 633 nm, suggests a direct correlation between the activation of the mode at 700 cm^{-1} and the background, which cannot be only related to fluorescence. Moreover, by acquiring the Raman spectra of T-horex@Au samples obtained by doubling the thickness of the Au layer (from 8 to 16 nm) we observe a significant reduction of the relative intensity of the mode at 700 cm^{-1}, together with a corresponding reduction of the background (Figure 4d).

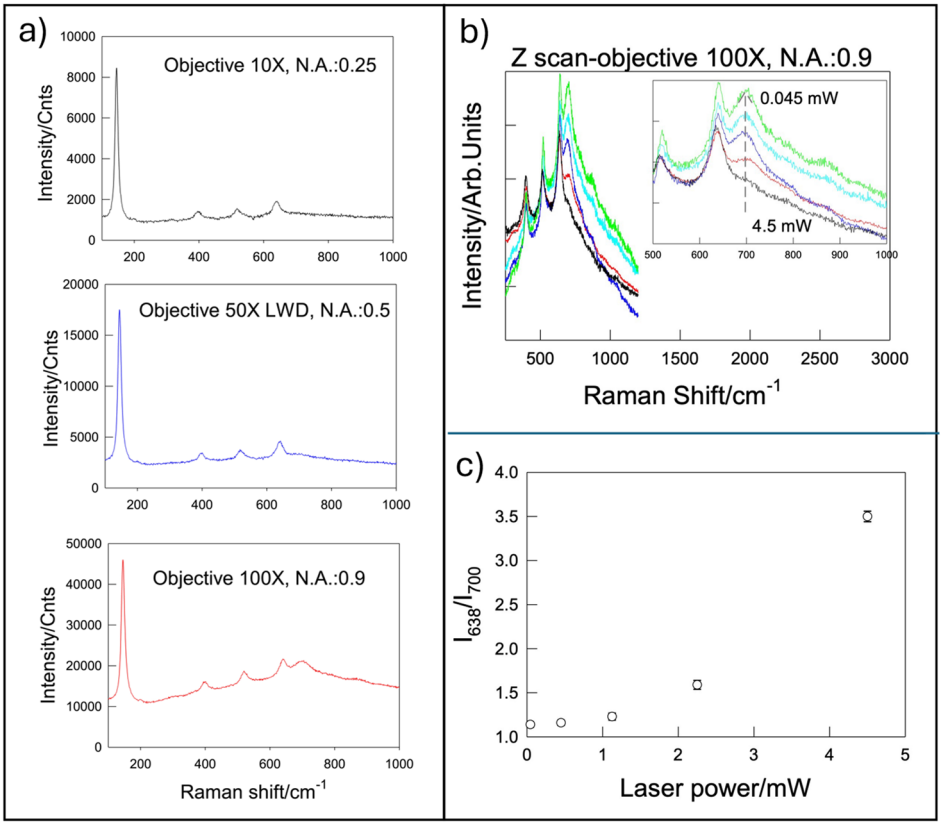

Figure 3. (**a**): Comparison among the spectra acquired on the same T-horex@Au with different microscope objectives at the same exposure time (10 s) with a 632.8 nm He-Ne laser at a power of 0.45 mW. (**b**): Optical Z-scan achieved by irradiating the same T-horex@Au bead with a He-Ne 632.8 nm source by progressively attenuating the power from 4.5 to 0.045 mW, with the following intervals: 4.5 mW; 2.25 mW; 1.125 mW; 0.45 mW, 0.045 mW. The exposure times at the different level of power were ruled to maintain the same number of photons on the sample surface (1.43×10^{16}) in each acquisition. (**c**): I_{638}/I_{700} cm^{-1} ratio as a function of the laser power.

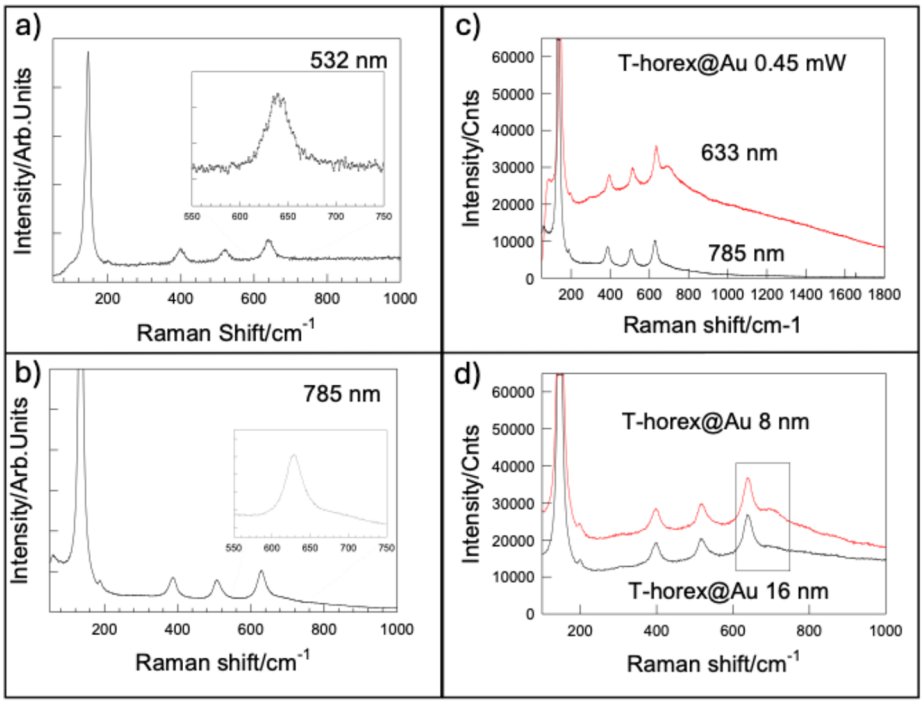

Figure 4. Raman spectra of T-horex@Au acquired at 532 nm (**a**) and 785 nm (**b**). (**c**) shows a comparison of the Raman spectra acquired at the same attenuated power at 632.8 and 785 nm, respectively (see Figure 3 and Experimental Section for details). (**d**) shows a comparison between the Raman spectra of T-horex@Au at two different thickness of gold shell (8 and 16 nm, respectively).

3.2. Discussion on the Origin and Nature of the Mode at 700 cm^{-1}

The data emerging from confocal microRaman experiments allow to draft some hypotheses on the origin of the mode at 700 cm^{-1}. At first sight, the fact that the intensity of this mode is correlated to the enhancement of the spectral background might suggest a direct dependence on gold photoluminescence (PL), which originates from the photo-induced excitation of d-electrons into the sp band, which leaves the corresponding holes into the d band. The following relaxation proceeds to the final recombination of the electron-hole pairs, with the emission of photons. These photons concur to give rise to the background observed in the Raman spectra. In particular, the energy gap associated to the d-sp interband transition at the X point of the Au Brillouin zone is 1.8 eV, which can be overcome by irradiating with a laser at 632.8 nm (1.96 eV). However, the intensity of PL should correlate to the energy of the laser utilized for the excitation. The fact that the spectral background observed by exciting the T-horex@Au beads with a laser energy of 2.33 eV (532 nm) is lower than that observed for the excitation at 1.96 eV (632.8 nm) can be justified only by a plasmon-induced enhancement of PL emission. This hypothesis can be corroborated also by noticing that the spectral background observed for excitation at 785 nm (1.58 eV) is weaker than that achieved at 632.8 nm, but stronger than that at 532 nm.

Literature reports several studies that demonstrate the possibility to modulate the intensity of PL by tuning the optical resonances of gold, playing with surface roughness of thin films and size/shape of particles [22]. Although visible spectra do not allow to directly detect surface plasmon resonances in T-horex@Au specimens, since the contribution of T-horex substrate dominates the optical response in the far field (Supporting Information Figure S4), the frequency of surface plasmon resonance in the near field could be at the origin of this enhanced PL at intermediate energy excitations. However, while the spectral background is directly dependent on PL, the mode at 700 cm^{-1} cannot be directly associated to the presence of gold. In fact, this mode is absent in glass substrates coated with the same thickness of Au, which still exhibit a strong PL background (Supporting Information Figure S5). These experimental data suggest that the TiO_2 substrate could play a major role, even though TiO_2 alone does not show any mode at 700 cm^{-1}, as shown by the confocal Raman spectra of T-horex. A possible explanation of the origin of this mode can be drawn through a more detailed investigation of the anatase Raman modes. Anatase belongs to the D_{4h} point group, giving rise to 6 possible phonon modes: A_{1g}, $2B_{1g}$, $3E_g$, B_{2u}, A_{2u}, $2E_u$. Among those, only the first three (A_{1g}, $2B_{1g}$ and $3E_g$) are Raman allowed, whereas the other three are symmetry forbidden. This prediction is valid for bulk phases. However, the symmetry of the surface is lowered to C_{2v}, which enables A_{2u} and E_u modes to be detected. Pioneering studies reporting the HREELS analysis of TiO_2 showed that a broad signal originated from the combination of A_{2u} and $E_u(2)$ modes appear around 662 nm (1.87 eV) [23,24]. Since this energy value perfectly matches that of the mode under investigation, we can associate it with the excitation of TiO_2 surface phonon modes. This would justify the ensemble of experimental observations discussed above. In the absence of gold (T-horex samples) the contribution of surface phonon modes to the Raman spectrum is negligible, as most of the signal comes from lattice phonons of bulk TiO_2. In the presence of gold (T-horex@Au) the signal of bulk TiO_2 is strongly attenuated, since most of the photons are shielded by the gold coating and spend most of the time on the sample surface. The surface plasmon polaritons propagate their evanescent field at the TiO_2 interface, stimulating the interaction with surface phonons and allowing their detection. The dependence of the surface phonon signal relative intensity on the power of the laser is a consequence of this pathway. At high laser power, the ratio of the photons that can reach the bulk phase is higher than that at low power. This means that at low power there are less photons, yet more localized at the surface, which increases the intensity of the surface phonon modes in comparison to that of bulk modes (Figure 5).

On the other hand, for thicker gold layers (i.e., 16 nm instead of 8 nm), the elastic backscattering of the light is too strong to allow for an efficient coupling with the TiO_2 surface phonon modes. For that reason, the attenuation of the photon flux in samples with a thicker layer of gold does not result in a significant enhancement of the surface phonon mode intensity. Finally, the fact that no modes at 700 cm^{-1} are observed on glass substrates coated with a gold layer with the same thickness of that of T-horex@Au, confirms that TiO_2 is necessary to generate this spectral feature. From another viewpoint, the fact that the observation of this surface mode requires an optimal combination of laser energy and thickness of the gold layer suggests that it can be taken as an internal reference for a direct tracking and diagnostics of surface plasmon polaritons within the T-horex@Au beads. However, this opportunity can be further extended for useful practical applications in Raman spectroscopy and, more generally, light-driven surface reactions. In fact, tuning the optical setup for maximizing the excitation of surface phonon modes entails the achievement of conditions that maximize light-matter interaction at the sample surface. Thus, the direct monitoring of this mode as an optical internal standard would allow to enhance the sensitivity of SERS experiments or optimize light management for driving surface photoreactions.

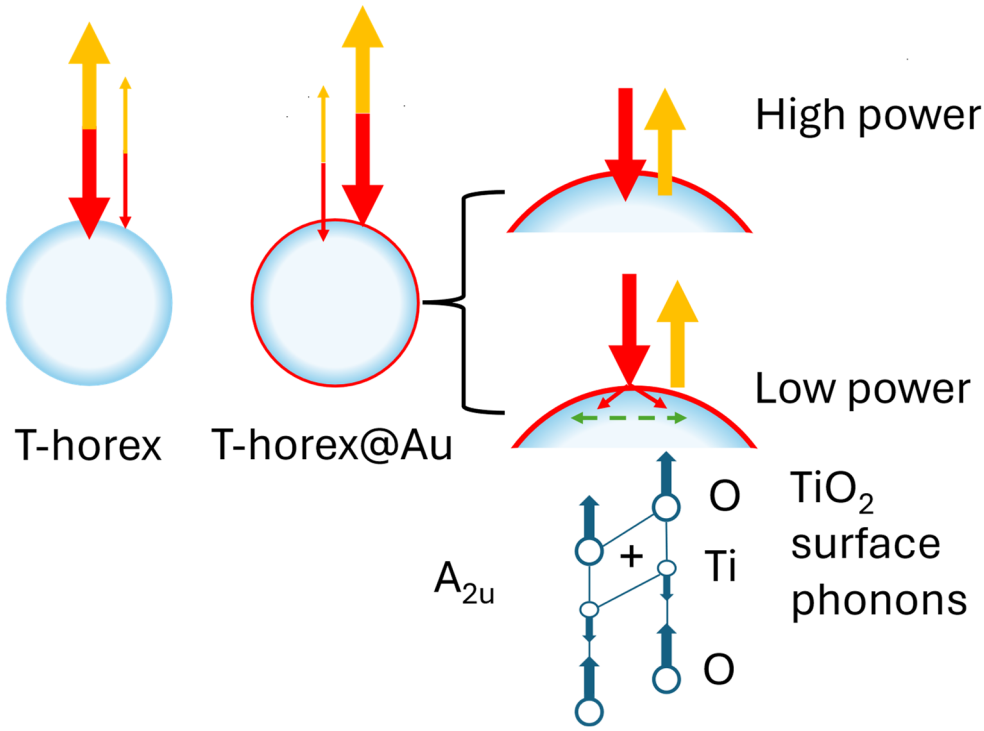

Figure 5. Scheme of the effects observed by acquiring the Raman spectrum of T-horex and T-horex@Au. The presence of Au allows for a more efficient confinement of light at the surface of the samples. In the case of low power irradiation, light trapping at the surface is strongly enhanced, allowing to detect the surface phonon modes of TiO_2. See the main text for details.

3.3. Proof-of-Concept: Optimization of SERS Experiments Guided by Surface Phonons Self-Diagnosis

As discussed above, the possibility of observing a spectral feature associated to the excitation of surface plasmon-polaritons can be conveniently exploited for both Raman and photocatalytic purposes. For example, acquiring Raman spectra with an optical setup that promotes coupling of light with surface modes could help to optimize SERS, extending detection limits and improving sensitivity.

This option was tested through a proof-of-concept experiments aimed at contrasting the performances of T-horex@Au with those achieved using the same layer of Au (8 nm) deposited on a glass slide substrate, under the same experimental conditions. As discussed before, the Raman spectra of Au-on-glass do not exhibit any surface mode at 700 cm^{-1}, which confirms the hypothesis of the excitation of TiO_2 surface phonons in the case of T-horex@Au.

Both T-horex@Au and Au-on-glass substrates were simultaneously soaked in the same 10^{-4} M L-cysteine aqueous solution (see experimental details) to promote the formation of a chemical bond between the thiol groups of L-cysteine and gold. This experimental protocol was utilized to ensure that the same amount of L-cysteine units has been bound on the gold layers, allowing a proper, quantitative comparison between the Raman sensitivity of the two substrates.

The Raman spectra were acquired using an optical setup optimized for the excitation of the surface plasmon-polariton mode, which should maximize the interaction between light and the analytes anchored on the Au surface. In these conditions, the Au-on-glass substrates did not show any spectral features of L-Cysteine, indicating that the simple deposition of a gold layer on glass is not sufficient to enhance the Raman response (Figure 6). On the other hand, the T-horex@Au substrate exhibited a Raman signal characterized by a strong background, yet allowing the detection of L-cysteine. The almost complete abatement of the intensity of -SH stretching mode in the 2500–2600 cm^{-1} region confirms the formation of S-Au bonds and successful removal of most of the excess of L-Cysteine molecules, which is further corroborated by the shift of $-CH_2$ stretching modes observed in the 2800–3000 cm^{-1} region. Moreover, the high intensity of these modes suggests that the detection limit could be further extended.

The fact that the experimental data have been acquired exactly at the same conditions highlights the key role of the TiO_2 substrate in managing light at the nanoscale. The plasmon-mediated excitation of surface phonons provides a direct, very effective tool for amplifying the interaction of the exciting light with surface adsorbates.

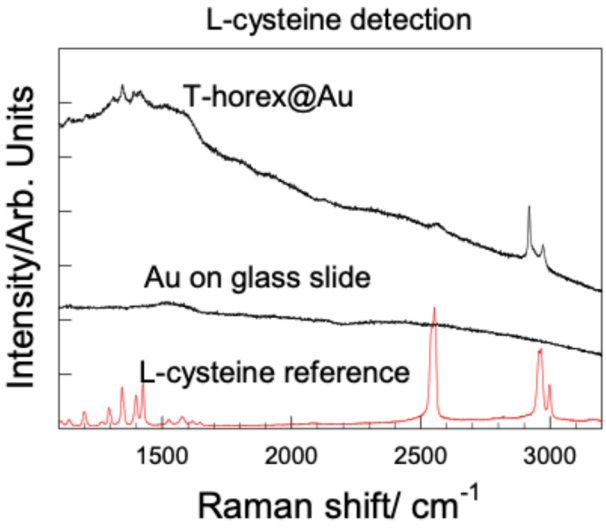

Figure 6. Optimized SERS detection of L-cysteine using T-horex@Au substrates. The Raman spectra on T-rex@Au substrates were acquired with a 632.8 nm He-Ne laser at a power of 1.125 mW, objetive 100X N.A.: 0.9. The Raman spectra of L-cysteine powder and L-cysteine deposited in glass slides coated with Au (8 nm, same thickness as T-horex@Au) are shown as a reference.

4. Conclusions

This study reports the first evidence of plasmon-mediated excitation and detection of TiO_2 surface phonon modes, which are forbidden in bulk phases. Although further studies are needed to elucidate the details on the activation mechanism, the confocal microRaman analysis demonstrated that an efficient confinement of light at the Au/TiO_2 interface enhances the sensitivity towards these modes, which become allowed by taking advantage of the interfacial lowering of symmetry. These modes can be utilized as internal standard for tracking and evaluating the quality of excitation of surface plasmon polaritons. Leveraging on this option, we demonstrated that the Raman enhancement achieved by the same metallic layer strongly depends on the substrate, and the intensity of the TiO_2 surface mode can be exploited to maximize/tune the amplification of Raman response. These results could allow to easily fabricate SERS substrates on a large scale and quickly optimize the setup of Raman experiments in metal/TiO_2 hybrid systems. In perspective, this approach could be extended to the management of surface plasmon-driven reactions [25] and promotion of enhanced photochemistry [26,27].

Supplementary Materials

The additional data and information can be downloaded at: https://media.sciltp.com/articles/others/260506172333397 2/PS-25120112-SI.pdf. Figure S1: Raman spectra of T-horex@Au acquired with a 0.5 N.A. objective as a function of the power attenuation. Figure S2: Temporal stability of the 700 cm^{-1} mode. Figure S3: Background-subtracted Raman spectra of Z-scan experiments and evolution of the 700 cm^{-1} mode. Figure S4: Far-field Vis reflectance of T-horex and T-horex@Au. Figure S5: Raman spectrum of Au (8 nm) on glass slide substrates.

Funding

This work was supported by the HOTMETA project under the PRIN 2022 MUR program funded by the European Union—Next Generation EU—PNRR—M4C2, investimento 1.1—"Fondo PRIN 2022"—HOT-carrier METasurfaces for Advanced photonics (HOTMETA), contract no. 2022LENW33—CUP: D53D2300229 0006.

Institutional Review Board Statement

Not applicable.

Informed Consent Statement

Not applicable.

Data Availability Statement

All data are available upon request.

Conflicts of Interest

The author declares no conflict of interest.

Use of AI and AI-Assisted Technologies

No AI tools were utilized for this paper.

References

1. Stiles, P.L.; Dieringer, J.A.; Shah, N.C.; et al. Surface-enhanced Raman spectroscopy. *Annu. Rev. Anal. Chem.* **2008**, *1*, 601–626. https://doi.org/10.1146/annurev.anchem.1.031207.112814.
2. Vassalini, I.; Rotunno, E.; Lazzarini, L.; et al. "Stainless" gold nanorods: Preserving shape, optical properties, and SERS activity in oxidative environment. *ACS Appl. Mater. Interfaces* **2015**, *7*, 18794–18802.
3. Stefancu, A.; Aizpurua, J.; Alessandri, I.; et al. Impact of surface enhanced Raman spectroscopy in catalysis. *ACS Nano* **2024**, *18*, 29337–29379.
4. Liu, X.; Ye, M.; Zhang, S.; et al. Enhanced photocatalytic CO_2 valorization over TiO_2 hollow microspheres by synergetic surface tailoring and Au decoration. *J. Mater. Chem. A* **2018**, *6*, 24245–24255.
5. Xu, T.; Jia, B.; Yan, K.; et al. Boosting visible light photocatalytic oxidation of CO using Au nanocatalysts through synergistic preparation of an Fe-doped TiO_2 support and cold plasma treatment. *Catal. Sci. Technol.* **2025**, *15*, 2844–2851.
6. Mahdavi-Shakib, A.; Sempel, J.; Hoffman, M.; et al. Au/TiO_2-Catalyzed Benzyl Alcohol Oxidation on Morphologically Precise Anatase Nanoparticles. *ACS Appl. Mater. Interfaces* **2021**, *13*, 11793–11804. https://doi.org/10.1021/acsami.0c20442.
7. Xu, Q.; Liu, Z. Studies on Photocatalytic Degradation for Organic Pollutants by TiO_2/Au Composite and its Antibacterial Properties. *Theor. Found. Chem. Eng.* **2023**, *57*, 1610–1617.
8. Reichert, R.; Jusys, Z.; Behm, R.J. Au/TiO_2 Photo(electro)catalysis: The Role of the Au Cocatalyst in Photoelectrochemical Water Splitting and Photocatalytic H_2 Evolution. *J. Phys. Chem. C* **2015**, *119*, 24750–24759.
9. Wang, K.; Lu, J.; Lau, C.H.; et al. Unravelling the C-C coupling in CO_2 photocatalytic reduction with H_2O on Au/TiO_{2-x}: Combination of plasmonic excitation and oxygen vacancy. *Appl. Catal. B Environ.* **2021**, *292*, 120147.
10. Ben-Jaber, S.; Peveler, W.J.; Quesada-Cabrera, R.; et al. Photo-induced enhanced Raman spectroscopy for universal ultra-trace detection of explosives, pollutants and biomolecules. *Nat Commun.* **2016**, *7*, 12189. https://doi.org/10.1038/ncomms12189.
11. Alessandri, I. Enhancing Raman scattering without plasmons: Unprecedented sensitivity achieved by TiO_2 shell-based resonators. *J. Am. Chem. Soc.* **2013**, *135*, 5541–5544.
12. Bontempi, N.; Vassalini, I.; Alessandri, I. All-dielectric core/shell resonators: From plasmon-free SERS to multimodal analysis. *J. Raman Spectrosc.* **2018**, *49*, 943–953.
13. Alessandri, I.; Carletti, L.; Ferroni, M.; et al. Bioinspired self-similar all-dielectric antennas: Probing the effect of secondary scattering centres by Raman spectroscopy. *Mater. Adv.* **2020**, *1*, 2443–2449.
14. Bontempi, N.; Carletti, L.; De Angelis, C.; et al. Plasmon-free SERS detection of environmental CO_2 on TiO_2 surfaces. *Nanoscale* **2016**, *8*, 3226–3231.
15. Alessandri, I.; Lombardi, J.R. Enhanced Raman scattering with dielectrics. *Chem. Rev.* **2016**, *116*, 14921–14981.
16. Boontanom, A.; Moscolari, L.; Kozma, E.; et al. Poly (dopamine)-coated TiO_2/SiO_2 resonators for the non-plasmonic SERS detection of organic analytes. *Appl. Surf. Sci.* **2026**, *720*, 165249. https://doi.org/10.1016/j.apsusc.2025.165249.
17. Salmistraro, M.; Schwartzberg, A.; Bao, W.; et al. Triggering and monitoring plasmon-enhanced reactions by optical nanoantennas coupled to photocatalytic beads. *Small* **2013**, *9*, 3301–3307.
18. Kadkhodazadeh, S.; Rosenkrantz de Lasson, J.; Beleggia, M.; et al. Scaling of the Surface Plasmon Resonance in Gold and Silver Dimers Probed by EELS. *J. Phys. Chem. C* **2014**, *118*, 5478–5485. https://doi.org/10.1021/jp500288s.
19. Garcia de Abajo, F.J. Optical excitations in electron microscopy. *Rev. Mod. Phys.* **2010**, *82*, 209–275.
20. Mooradian, A. Photoluminescence of metals. *Phys. Rev. Lett.* **1969**, *22*, 185–187.
21. Boyd, G.T.; Yu, Z.H.; Shen, Y.R. Photoinduced luminescence from the noble metals and its enhancement on roughened surfaces. *Phys. Rev. B* **1986**, *33*, 7923–7936.
22. Ngoc, L.L.T.; Wiedemair, J.; van den Berg, A.; et al. Plasmon-modulated photoluminescence from gold nanostructures and its dependence on plasmon resonance, excitation energy, and band structure. *Opt. Express* **2015**, *23*, 5547–5564. https://doi.org/10.1364/OE.23.005547.
23. Durinck, G.; Poelman, H.; Clauws, P.; et al. Observation of surface phonons on the (001) and (100) surfaces of anatase minerals. *Solid State Commun.* **1991**, *80*, 579–581. https://doi.org/10.1016/0038-1098(91)90155-O.
24. Poelman, H.; Fiermans, L. Surface Phonon Spectra of Mineral TiO_2 Anatase (001) and (100). *Surf. Sci. Spectra* **1998**, *5*, 252–256. https://doi.org/10.1116/1.1247845.
25. Alessandri, I.; Ferroni, M.; Depero, L.E. Plasmon-Assisted, Spatially Resolved Laser Generation of Transition Metal Oxides from Liquid Precursors. *J. Phys. Chem. C* **2011**, *115*, 5174–5180. https://doi.org/10.1021/jp110324y.

26. Alessandri, I. 4-Aminothiophenol Photodimerization without Plasmons. *Angew. Chem. Int. Ed.* **2022**, *61*, e202205013. https://doi.org/10.1002/anie.202205013.
27. Alessandri, I.; Vassalini, I. Oxygen-mediated surface photoreactions: Exploring new pathways for sustainable chemistry. *ChemPhotoChem.* **2023**, *7*, e202300069. https://doi.org/10.1002/cptc.202300069.